DOI: 10.1021/ic100360n

Inorganic Chemistry
Article

$Rb_{16}Cd_{25.39(3)}Sb_{36}$: An Electron-Deficient Zintl Phase Containing Infinite Dodecahedron Chains

Wu-Zui Zheng,[†,‡] Peng Wang,[†,‡] Li-Ming Wu,[†] Yi Liu,[†] and Ling Chen*[,†]

[†]*Key Laboratory of Optoelectronic Materials Chemistry and Physics, Fujian Institute of Research on the Structure of Matter, Chinese Academy of Sciences, Fuzhou, Fujian 350002, People's Republic of China, and* [‡]*Graduate School of the Chinese Academy of Sciences, Beijing 100039, People's Republic of China*

Received February 22, 2010

A novel ternary antimonide $Rb_{16}Cd_{25.39(3)}Sb_{36}$ has been synthesized by a solid-state reaction of the appropriate amount of elements in a welded niobium tube at 530 °C. The compound crystallizes in orthorhombic space group *Cmcm* (No. 63) with $a = 16.499(5)$ Å, $b = 12.391(4)$ Å, $c = 12.400(4)$ Å, and $Z = 1$. The structure features a new 3D network constructed of chains of Rb^+-centered dodecahedra running along [001]. The atomic distribution of the Cd_8Sb_{12} dodecahedron presents an energetically favored pattern without any Cd−Cd bonding. The formation of the phase and the occurrence of a very narrow phase width of $Rb_{16}Cd_{24+x}Sb_{36}$ [$0.94(2) \le x \le 1.47(3)$] have been studied in detail. The Fermi level of the title compound is expected to be located between those of the hypothetical models of "$[Rb_{16}Cd_{24}Sb_{36}]^{0}$" (I, poor metallic) and "$[Rb_{16}Cd_{24}Sb_{36}] + 4e$" (II, narrow-band-gap semiconductor), which agrees well with the experimental measurements. In the temperature range of 300−473 K, the as-synthesized $Rb_{16}Cd_{25.39(3)}Sb_{36}$ exhibits p-type semiconductor behavior and shows temperature-independent thermal conductivities (around 0.49 W/m·K). The electrical conductivity, Seebeck coefficient, and figure of merit (ZT) of $Rb_{16}Cd_{25.39(3)}Sb_{36}$ are temperature-dependent; these values are 57.4 S/cm, +81.4 μV/K, and 0.04, respectively, at 466 K.

Introduction

Compounds featuring cages that accommodate the alkali or alkaline-earth metal atoms have widely attracted research interest as possible promising thermoelectric (TE) materials.[1−3] Such accommodated ions, so-called guest ions or rattling atoms, contribute greatly to the low lattice thermal conductivity through scattering of the acoustic phonons that carry heat.[4−6] Type I clathrate is a well-known caged structure that has a general formula of $A_8B_xC_{46-x}$ (A = alkali, alkaline-earth, or rare-earth metal; B = Al, Ga, In, Zn, and Cd; C = Si, Ge, and Sn). The main structural motif of a clathrate is the complex 3D network constructed from chains of 24-atom tetrakaidecahedra sharing both trans hexagonal faces and chains of the intervening 20-atom dodecahedra that share pentagonal faces with the tetrakaidecahedron chains. The TE property studies indicate that some of the type I clathrate compounds have exhibited superior TE properties; for example, $Yb_{0.5}Ba_{7.5}Ga_{16}Ge_{30}$ has $ZT = 1.1$ at 950 K[7] and a higher $ZT = 1.35$ for $Ba_8Ga_{16}Ge_{30}$ at 900 K;[8] both values are comparable with that of the best commercial TE materials. Recently, our group has reported the first two examples of an antimony-based type I clathrate, $Cs_8M_{18}Sb_{28}$ (M = Zn and Cd),[9] whose skeleton is constructed by Sb atoms as the main components and Cd or Zn atoms as the second components. Other reports have indicated that some Sb-based compounds have exhibited very good TE properties; for instance, $Yb_{14}MnSb_{11}$ has a ZT of ∼1.0 at 1223 K,[10] filled skutterudeite $Yb_{0.19}Co_4Sb_{12}$ shows $ZT = 1.14$ at 640 K,[11a] $CoSb_3$ has $ZT = 0.04$, $Yb_{0.02}Co_4Sb_{12}$ has $ZT = 0.3$ at 300 K,[11b] and β-Zn_4Sb_3 reaches $ZT = 1.3$ at 650 K.[12] Therefore, the investigation on the

*To whom correspondence should be addressed. E-mail: chenl@fjirsm.ac.cn. Tel: (011)86-591-83704947.

(1) Nolas, G. S.; Weakley, T. J. R.; Cohn, J. L. *Chem. Mater.* **1999**, *11*, 2470–2473.
(2) Sales, B. C.; Chakoumakos, B. C.; Jin, R.; Thompson, J. R.; Mandrus, D. *Phys. Rev. B* **2001**, *63*(24), 245113.
(3) Kim, S. J.; Kanatzidis, M. G. *Inorg. Chem.* **2001**, *40*, 3781–3785.
(4) Nolas, G. S.; Slack, G. A.; Morelli, D. T.; Tritt, T. M.; Ehrlich, A. C. *J. Appl. Phys.* **1996**, *79*, 4002–4008.
(5) Cohn, J. L.; Nolas, G. S.; Fessatidis, V.; Metcalf, T. H.; Slack, G. A. *Phys. Rev. Lett.* **1999**, *82*, 779–782.
(6) Nolas, G. S.; Cohn, J. L.; Slack, G. A.; Schujman, S. B. *Appl. Phys. Lett.* **1998**, *73*, 178–180.
(7) Tang, X. F.; Li, P.; Deng, S. K.; Zhang, Q. J. *J. Appl. Phys.* **2008**, *104*, 013706.
(8) Saramat, A.; Svensson, G.; Palmqvist, A. E. C.; Stiewe, C.; Mueller, E.; Platzek, D.; Williams, S. G. K.; Rowe, D. M.; Bryan, J. D.; Stucky, G. D. *J. Appl. Phys.* **2006**, *99*, 023708.
(9) Liu, Y.; Wu, L. M.; Li, L. H.; Du, S. W.; Corbett, J. D.; Chen, L. *Angew. Chem., Int. Ed.* **2009**, *48*, 5305–5308.
(10) Brown, S. R.; Kauzlarich, S. M.; Gascoin, F.; Synder, G. J. *Chem. Mater.* **2006**, *18*, 1873–1877.
(11) (a) Nolas, G. S.; Kaeser, M.; Littleton, R. T. I.; Tritt, T. M. *Appl. Phys. Lett.* **2000**, *77*, 1855–1857. (b) Imai, H.; Shimakawa, Y.; Kubo, Y. *Phys. Rev. B* **2001**, *64*, 244104.
(12) Chitroub, M.; Besse, F.; Scherrer, H. *J. Alloys Compd.* **2008**, *460*, 90–93.

Published on Web 05/28/2010

Table 1. Parallel Reactions with Different Loading Ratios [Rb:Cd:Sb = 16:*y*:36 (*y* = 20−32)] and Phase Analyses of the Corresponding Products[a]

sample	*y*	phase identity	XRD pattern
1	20[b]	A[c] + unknown (trace)	Figure S2a in the SI
2	21	A + unknown (trace)	Figure S2b in the SI
3	22	A (major) + unknown (minor)	Figure S2c in the SI
4	23[b]	A + unknown (trace)	Figure S2d in the SI
5	24[b]	A (pure phase)	Figures 1 and S2e in the SI
6	25[b]	A (major) + B[c] (trace)	Figure S2f in the SI
7	25, 39	A (major) + B (minor)	Figure S1 in the SI
8	26[b]	A (major) + B (minor)	Figure S3a in the SI
9	29	A (50%) + B (50%)	Figure S3b in the SI
10	32	A (minor) + B (major)	Figure S3c in the SI

[a] The overall loading of each reaction is 300 mg. For example, for a reaction with Rb:Cd:Sb = 16:20:36, 0.6 mmol of Rb, 0.75 mmol of Cd, and 1.35 mmol of Sb were weighed. The heating profile of each reaction is as follows: heated at 530 °C for 160 h and subsequently cooled to room temperature over 140 h. [b] Although single crystals generated by these reactions have different stoichiometries according to the single-crystal XRD data listed in Table 5, the deviations on the corresponding powder XRD patterns are not detectable (Table 6). For phase analysis, the calculated pattern of $Rb_{16}Cd_{25.39(3)}Sb_{36}$ is used as the standard for all phase analyses in this paper. [c] A: $Rb_{16}Cd_{25.39(3)}Sb_{36}$. B: $Rb_2Cd_5Sb_4$.[13]

novel Sb-based caged compounds is our main research interest, and our efforts have led to the discovery of $Rb_{16}Cd_{25.39(3)}Sb_{36}$, whose anionic framework comprises parallel infinite chains of alkali-metal-centered dodecahedra. The synthesis, crystal structure, electrical and thermal transport properties, and electronic structure are reported in this paper.

Experimental Section

Syntheses. All manipulations were performed inside an Ar-filled glovebox with controlled O_2 and moisture levels below 0.1 ppm. The following reactants were used as purchased and stored in the glovebox. Rb (99.9%) was purchased from Alfa Aesar China Co., Ltd. (Tianjin, China). Sb (granular, 99.99%) and Cd (granular, 99.999%) were purchased from Sinopharm Chemical Reagent Co., Ltd. The title compound $Rb_{16}Cd_{25.39(3)}Sb_{36}$ was first identified as a minor second phase in the synthesis aiming at a hypothetical clathrate "$Rb_8Cd_{18}Sb_{28}$". The reactant mixture of Rb, Cd, and Sb with an overall loading amount of 300 mg was loaded in a welded Nb tube that was sealed in an evacuated quartz tube under vacuum at 10^{-3} Pa. The samples were heated at 530 °C for 160 h and subsequently cooled to room temperature over 140 h. The gray powdery products contained a few gray-black needle crystals with a metallic shine that were stable in air over a period of weeks. The powder X-ray diffraction (XRD) pattern of the gray powdery product indicated a major phase of $Rb_2Cd_5Sb_4$ (Supporting Information, Figure S1),[13] but the single-crystal XRD indicated that the gray-black needle crystals were $Rb_{16}Cd_{25.39(3)}Sb_{36}$. Then a stoichiometric reaction was performed, and the product was $Rb_{16}Cd_{25.39(3)}Sb_{36}$ plus a minor impurity of the Cd-rich compound $Rb_2Cd_5Sb_4$.[13] Apparently, Rb and Sb had been lost by reaction with the Nb tubing, because after the reaction, the Nb tubing was fragile, and some "sheets" from the inner wall could be easily peeled off and were identified as $NbSb_2$ by XRD. Subsequently, a new reaction of Rb:Cd:Sb = 16:24:36 was loaded with excess Rb and Sb amounts (Table 1, sample **5**). The assembly was heated with the same heating profile as that described above; a pure $Rb_{16}Cd_{25.39(3)}Sb_{36}$ phase was obtained according to XRD analysis (Figure 1).

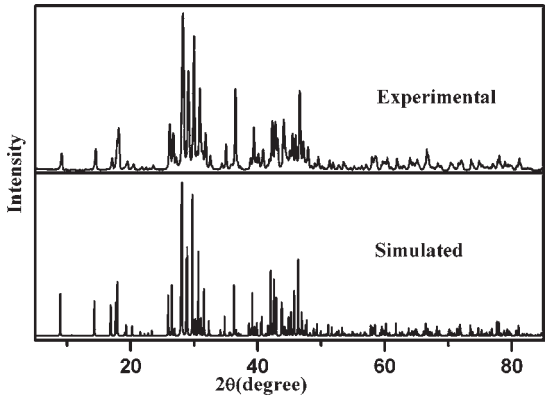

Figure 1. Experimental and simulated powder XRD patterns of $Rb_{16}Cd_{25.39(3)}Sb_{36}$ synthesized at 530 °C.

Unfortunately, parallel reactions with other combinations, such as Cs/Cd/Sb or A/Zn/Sb (A = Rb and Cs), only generated the Cd-rich compound $Cs_2Cd_5Sb_4$[13] or type I clathrate $A_8M_{18}Sb_{28}$ (A = Rb and Cs; M = Cd and Zn).[9,14]

In order to probe the possible phase width, we tried 10 parallel reactions with different loading ratios, by which the amount of Cd (*y*) was changed from 78.8% to 126% of the single-crystal-refined stoichiometry (Rb:Cd:Sb = 16:25.4:36). The corresponding reaction conditions and the phase analyses are listed in Table 1, and the XRD patterns are shown in the Supporting Information, Figures S2 and S3. A detailed discussion can be found in the following section.

Meanwhile, the annealing temperature effect was investigated. Three parallel reactions with identical loading ratios of Rb:Cd:Sb = 16:24:36 (see sample **5** in Table 1) were carried out at different annealing temperatures of 520, 530, and 550 °C, respectively. The corresponding XRD patterns are shown in the Supporting Information, Figure S4. The results revealed that the formation of $Rb_{16}Cd_{25.39(3)}Sb_{36}$ was sensitive to the annealing temperature. A reaction heated at a temperature 10 °C lower than the optimal 530 °C generated a mixture containing a second type I clathrate $Rb_8Cd_{18}Sb_{28}$ phase.[14] A reaction heated at 20 °C higher produced the Cd-rich phase $Rb_2Cd_5Sb_4$[13] as the major product. A detailed description is listed below.

Single-Crystal XRD. A gray-black needle crystal of 0.20 × 0.12 × 0.10 mm^3 from sample **5** was mounted on a glass fiber. The single-crystal XRD data were collected on a Rigaku Mercury CCD diffractometer equipped with a graphite-monochromated Mo Kα radiation source (λ = 0.710 73 Å) at 293 K. The absorption corrections were done by the multiscan method.[15] The space group was determined to be *Cmcm* (No. 63) according to the systematic absence, *E*-value statistics, and subsequent successful refinement of the crystal structure. The structure was solved by direct methods and refined by a full-matrix least-squares fitting on F^2 by *SHELX-97*.[16] The assignments of Rb, Cd, and Sb were determined on the basis of the interatomic distances and relative displacement parameters. All of the atoms were refined with anisotropic thermal parameters and a secondary extinction correction. The final atomic positions were standardized with the *TIDY* program. The Cd3 site was first refined with full occupancy, which resulted in a very large atomic displacement parameter of 0.312 $Å^2$ in comparison with those of Cd1 (0.018 $Å^2$) and Cd2 (0.023 $Å^2$) and large *R* values of R1 = 0.0597 and wR2 = 0.2198. Subsequently, the occupancy of Cd3 was allowed to vary, and refinement generated a site

(13) (a) $Rb_2Cd_5Sb_4$: *Cmcm*, *a* = 13.1241(11) Å, *b* = 7.9998(5) Å, *c* = 13.1413(8) Å, *V* = 1379.71(17) $Å^3$, CSD 421453. (b) $Cs_2Cd_5Sb_4$: *Cmcm*, *a* = 13.1704(9) Å, *b* = 8.0153(7) Å, *c* = 13.2434(11) Å, *V* = 1398.04(19) $Å^3$, CSD 421451.

(14) $Rb_8Cd_{18}Sb_{28}$: $Pm\bar{3}n$, *a* = 12.1643(14) Å, *V* = 1800.0(4) $Å^3$, CSD 421454.

(15) Corp, R. *CrystalClear*, version 1.3.5; Woodlands, TX, 1999.

(16) Sheldrick, G. M. *SHELXL-97: Program for Crystal Structure Solution*; University of Göttingen: Göttingen, Germany, 1997.

Table 2. Crystallographic Data and Refinement Details for $Rb_{16}Cd_{25.39(3)}Sb_{36}$

empirical formula	$Rb_{16}Cd_{25.39(3)}Sb_{36}$
fw	8604.36
temperature (K)	293(2)
radiation, wavelength (Å)	Mo Kα, λ = 0.710 73
cryst syst	orthorhombic
space group, Z	*Cmcm*, 1
unit cell dimens (Å)	a = 16.499(5)
	b = 12.391(4)
	c = 12.400(4)
volume (Å^3)	2535.1(15)
calcd density (g/cm^3)	5.636
abs coeff (mm^{-1})	22.226
reflns collected/unique	9638/1572 [R(int) = 0.0371]
data/restraints/param	1572/0/62
GOF on F^2	1.192
final R indices [$I > 2\sigma(I)$][a]	R1 = 0.0259, wR2 = 0.0612
largest diff peak/hole (e/Å^3)	1.523/−2.149

[a] $R1 = \sum||F_o| - |F_c||/\sum|F_o|$, $wR2 = [\sum w(F_o^2 - F_c^2)^2/\sum w(F_o^2)^2]^{1/2}$.

Table 3. Atomic Coordinates, Equivalent Isotropic Displacement Parameters (Å^2), and Site Occupancies of $Rb_{16}Cd_{25.39(3)}Sb_{36}$

atom	Wyckoff position	x	y	z	U(eq)[a]	occupancy
Rb1	4*a*	0	0	0	0.027(1)	1
Rb2	4*c*	0	0.5712(1)	1/4	0.093(1)	1
Rb3	8*g*	0.1947(1)	0.3522(1)	1/4	0.034(1)	1
Cd1	8*g*	0.1399(1)	0.0537(1)	1/4	0.018(1)	1
Cd2	16*h*	0.3678(1)	0.2486(1)	0.0465(1)	0.022(1)	1
Cd3	8*e*	0.3890(2)	0	0	0.025(1)	0.174(3)
Sb1	4*c*	0	0.1919(1)	1/4	0.015(1)	1
Sb2	8*f*	0	0.3360(1)	0.0724(1)	0.017(1)	1
Sb3	8*g*	0.4150(1)	0.3377(1)	1/4	0.014(1)	1
Sb4	16*h*	0.2335(1)	0.0951(1)	0.0626(1)	0.017(1)	1

[a] U(eq) is defined as one-third of the trace of the orthogonalized U_{ij} tensor.

occupancy of 17.4(3)%, with a comparable displacement factor of 0.025 Å^2 and relatively low R values of R1 = 0.0259 and wR2 = 0.0629. The eventual formula was then refined as $Rb_{16}Cd_{25.39(3)}Sb_{36}$. Regarding the large displacement parameter on the Rb2 site, we have refined the occupancy, which converged at 99.4(8)% with an unchanged U(eq) = 0.092(1) and R1 = 0.0259 and wR2 = 0.0612. Such a treatment generated 0.174(3) occupancy on Cd3 as well. This refinement suggested that the Rb2 site was fully occupied. Second, we have split the Rb2 4*c* site into a pair of 8g and 8f sites. The split generated Rb2 8*f* with an occupancy of 0.20(3) and Rb22 8g with an occupancy of 0.30(3), R1 = 0.0256, and wR2 = 0.0614 and a Cd3 site occupancy of 0.174(3). Not surprisingly, the split gave similar U(eq) for four Rb atoms; however, the R values, the Cd3 site occupancy, and the overall formula were unchanged. Considering that the split generated a complex/confusing structural picture on the Rb2 site, we therefore reported the refinement results as listed in Table 2. On the other hand, the energy-dispersive X-ray (EDX) and inductively coupled plasma (ICP) analyses on the crystals obtained from sample **5** had excluded the possibility that the Cd3 site was occupied by Rb or Sb and, therefore, supported the partial occupancy on the Cd3 site indicated by the single-crystal data. The crystallographic data and structural refinements are summarized in Table 2. The atomic positions, anisotropic displacement parameters, and occupancy factors are provided in Table 3. The selected bond lengths and angles are listed in Table 4. Besides, five different single crystals from samples **1**, **4**−**6**, and **8**, respectively (Table 1) were also refined; they were $Rb_{16}Cd_{24.94(2)}Sb_{36}$, $Rb_{16}Cd_{25.03(2)}Sb_{36}$, $Rb_{16}Cd_{25.39(3)}Sb_{36}$, $Rb_{16}Cd_{25.47(3)}Sb_{36}$, and $Rb_{16}Cd_{25.46(3)}Sb_{36}$. The corresponding data are listed in Table 5 and Tables S1−3 in the Supporting Information.

Table 4. Selected Bond Lengths (Å) and Angles [deg] for $Rb_{16}Cd_{25.39(3)}Sb_{36}$

Cd1−Sb3	2.825(2)	Cd2−Sb2	2.8330(8)
Cd1−Sb4 (×2)	2.8374(8)	Cd2−Sb3	2.8626(9)
Cd1−Sb1	2.874(2)	Cd2−Sb4	2.8948(8)
Cd3−Sb2 (×2)	2.879(2)	Cd2−Sb4	2.9267(9)
Cd3−Sb4 (×2)	2.927(3)	Sb1−Sb2 (×2)	2.836(2)
Sb2−Cd2 (×2)	2.8330(8)	Sb1−Cd1	2.874(2)
Sb2−Cd3 (×2)	2.879(2)	Sb3−Sb3	2.804(2)
Sb4−Sb4	2.823(2)	Sb3−Cd1	2.825(2)
Sb4−Cd2	2.8948(8)	Sb3−Cd2	2.8626(9)
Sb3−Cd1−Sb4 (×2)	110.24(2)	Sb2−Cd2−Sb3	113.08(3)
Sb4−Cd1−Sb1	109.93(3)	Sb2−Cd2−Sb4	116.69(3)
Sb3−Cd1−Sb1	107.89(3)	Sb3−Cd2−Sb4	108.12(3)
Sb4−Cd1−Sb1 (×2)	109.24(2)	Sb2−Cd2−Sb4	112.21(3)
Sb2−Cd3−Sb2	101.0(2)	Sb3−Cd2−Sb4	113.35(2)
Sb2−Cd3−Sb4 (×2)	139.36(5)	Sb4−Cd2−Sb4	91.68(3)
Sb2−Cd3−Sb4 (×2)	110.85(3)	Sb2−Cd3−Sb4	57.66(7)

Powder XRD. The powder XRD patterns were taken at room temperature on a Rigaku MiniFlex II powder diffractometer with monochromatized Cu Kα radiation. Data were collected in the range of 2θ = 5−85° with a scan step of 0.01° with Si as the inner standard if mentioned. The data analyses were carried out with the aid of the *JADE 5.0* software package.

Elemental Analyses. The semiquantitative microprobe elemental analysis was performed on a field emission scanning electron microscope (JSM6700F) equipped with an energy-dispersive X-ray spectroscope (Oxford INCA) on the same single crystal of $Rb_{16}Cd_{25.39(3)}Sb_{36}$ for which the single-crystal XRD data were collected. The results indicated the presence of Rb, Cd, and Sb, and no heteroelement such as Nb was detected in any case. The EDX analyses gave average atomic percentages of 21.1(9)% Rb, 32.2(12)% Cd, and 46.7(9)% Sb, which were in good agreement with single-crystal refinement stoichiometry ($Rb_{16}Cd_{25.39(3)}Sb_{36}$ atomic percentage: 20.7% Rb, 32.8% Cd, and 46.5% Sb).

Meanwhile, the Ultima-2 inductively coupled plasma optimal emission spectrometer was used to quantitatively determine the composition of the hand-picked single crystals from sample **5**. The mass percentage of 32.6(6)% Cd and 50.9(10)% Sb also agreed well with the single-crystal refinement stoichiometry ($Rb_{16}Cd_{25.39(3)}Sb_{36}$ mass percentage: 33.2% Cd and 50.9% Sb).

Physical Property Measurements. The thoroughly ground polycrystalline sample was cold-pressed with a 769YP-15A compressor inside an Ar-filled glovebox with controlled O_2 and moisture levels below 0.1 ppm. The thermal diffusivity and heat capacity of $Rb_{16}Cd_{25.39(3)}Sb_{36}$ were measured on a thus-made disk (thickness, 1.64 mm; diameter, 10 mm; measured density, ~80% of the theoretical density) by laser flash techniques with a Netzsch LFA 457 system in an Ar atmosphere with pyroceram 9606 as the standard for heat capacity measurement. The Seebeck coefficient and electrical conductivity of a rectangular bar (8.64 × 3.14 × 1.64 mm^3) cut from the above-mentioned disk inside an Ar-filled glovebox was measured on a ULVAC ZEM-3 instrument from room temperature to 200 °C. Each curve was measured three times in the temperature range to ensure the stability and repeatability of the data. The thermal conductivity was calculated according to the equation $\kappa(T) = \alpha(T)\, C_p(T)\, \rho(T)$, in which $\rho(T)$ is the experimental density, $C_p(T)$ the heat capacity, and $\alpha(T)$ the measured thermal diffusivity.

Electronic Structure Calculations. The first principle calculations were performed using the L/APW+lo method,[17] as implemented in the WIEN2k code.[18] The Perdew−Burke−Ernzerhof[19]

(17) Madsen, G. K. H.; Blaha, P.; Schwarz, K.; Sjostedt, E.; Nordstrom, L. *Phys. Rev. B* **2001**, *64*(19), 195134.
(18) Blaha, P.; Schwarz, K.; Madsen, G. K. H.; Kvasnicka, D.; Luitz, J. *WIEN2k, An Augmented Plane Wave and Local Orbitals Program for Caculating Crystal Properties*; Technische Universität: Wien, Austria, 2001.
(19) Perdew, J. P.; Burke, K.; Ernzerhof, M. *Phys. Rev. Lett.* **1996**, *77*, 3865–3868.

Table 5. Selected Crystallographic Data and Refinement Details for the Corresponding Crystals from Different Reactions[a]

	1	**4**	**5**	**6**	**8**
empirical formula	$Rb_{16}Cd_{24.94(2)}Sb_{36}$	$Rb_{16}Cd_{25.03(2)}Sb_{36}$	$Rb_{16}Cd_{25.39(3)}Sb_{36}$	$Rb_{16}Cd_{25.47(3)}Sb_{36}$	$Rb_{16}Cd_{25.46(3)}Sb_{36}$
fw	8553.78	8563.89	8604.36	8613.35	8612.22
unit cell dimens (Å)[b]	a = 16.504(4)	a = 16.513(6)	a = 16.499(5)	a = 16.503(2)	a = 16.523(6)
	b = 12.411(3)	b = 12.413(4)	b = 12.391(4)	b = 12.3899(8)	b = 12.395(4)
	c = 12.380(3)	c = 12.395(4)	c = 12.400(4)	c = 12.4224(9)	c = 12.417(5)
volume (Å^3)	2535.7(11)	2540.7(15)	2535.1(15)	2540.0(3)	2542.9(16)
final R indices [$I > 2\sigma(I)$][c]	$R1$ = 0.0217	$R1$ = 0.0242	$R1$ = 0.0259	$R1$ = 0.0254	$R1$ = 0.0286
	$wR2$ = 0.0499	$wR2$ = 0.0525	$wR2$ = 0.0612	$wR2$ = 0.0569	$wR2$ = 0.0673
largest diff peak/hole (e/Å^3)	1.460/−1.222	1.206/−2.198	1.523/−2.149	1.235/−1.855	1.341/−1.682
site occupancy of Cd3	0.117(2)	0.129(2)	0.174(3)	0.184(3)	0.183(3)

[a] Detailed crystallographic data are available in the Supporting Information, Tables S1−S3. [b] Obtained from the single-crystal XRD data. [c] $R1 = \sum||F_o| - |F_c||/\sum|F_o|$, $wR2 = [\sum w(F_o^2 - F_c^2)^2/\sum w(F_o^2)^2]^{1/2}$.

and Engel−Vosko (EV) generalized gradient approximation (GGA) was used for the exchange-correlation potential because the EV-GGA has been proven to generate a better approximation of the band gap than GGA or the local density approximation.[20] The electronic configurations for Rb, Cd, and Sb were as follows: Rb, [Kr]5s^1; Cd, [Kr]4d^{10}5s^2; Sb, [Kr]4d^{10}5s^{2}5p^3. The values of the atomic radii (muffin-tin radii or RMT) were set to 2.5 au for all atoms, and a plane wave cutoff was set to $R_{mt} \times K_{max} = 7.0$. The scalar relativistic approximation for heavy elements was considered, with spin−orbit coupling neglected. The convergence of the self-consistent iterations was set to be within 0.0001 Ry for 18 k points inside the irreducible Brillouin zone with a cutoff of −6 Ry between the valence and core states.

Results and Discussion

Synthesis and Phase Width. The synthesis of the title compound is difficult. We think the reason may include the following points: (1) the unavoidable side reactions between Rb or Sb and the Nb tubing; (2) the existence of the competition phases, such as $Rb_2Cd_5Sb_4$[13] and type I clathrate $Rb_8Cd_{18}Sb_{28}$;[14] (3) the sensitivity to the annealing temperature; a 10−20° deviation from the optimal annealing temperature will cause formation of the competition phases. Fortunately, as listed in Table 1, 10 parallel reactions have proven that with the appropriate amount of compensation of Rb and Sb, pure-phased $Rb_{16}Cd_{25.39(3)}Sb_{36}$, can be produced (sample **5**). Samples **1**−**4** that have insufficient Cd with respect to the Rb:Cd:Sb = 16:24:36 ratio generate $Rb_{16}Cd_{25.39(3)}Sb_{36}$ as the main product, together with a minor unknown phase, while samples **6**−**10** with an excess amount of Cd generate a mixture of $Rb_{16}Cd_{25.39(3)}Sb_{36}$ and a Cd-rich compound $Rb_2Cd_5Sb_4$.[13] Samples **6**−**10** also show that in the produced mixture the relative percentage of Cd-rich $Rb_2Cd_5Sb_4$ phase[13] increases from a trace component (in **6**) to a major phase (in **10**) with an increase of the loading Cd amount.

Such Rb/Cd/Sb reactions are also temperature-sensitive. For example, three reactions with the identical loading ratios of Rb:Cd:Sb = 16:24:36 (see sample **5**) were carried out under the same experimental conditions except that they were annealed at 520, 530, and 550 °C, respectively. The XRD analyses shown in Supporting Information, Figure S4, indicate that the 520 °C reaction generates a mixture of $Rb_{16}Cd_{25.39(3)}Sb_{36}$ and type I clathrate $Rb_8Cd_{18}Sb_{28}$,[14] the 530 °C reaction generates a pure $Rb_{16}Cd_{25.39(3)}Sb_{36}$ phase, and the 550 °C reaction generates $Rb_2Cd_5Sb_4$[13] as the major phase.

(20) Engel, E.; Vosko, S. H. *Phys. Rev. B* **1993**, *47*, 13164–13174.

Table 6. Calculated Lattice Constants from the Powder XRD Patterns with Si as the Inner Standard

sample	a	b	c	V
1	16.498(2)	12.389(1)	12.401(2)	2534.7(10)
2	16.503(2)	12.388(2)	12.402(1)	2535.5(10)
3	16.494(2)	12.386(2)	12.403(3)	2533.9(14)
4	16.502(2)	12.388(1)	12.401(1)	2535.1(8)
5	16.501(2)	12.391(1)	12.401(1)	2535.6(8)
6	16.497(2)	12.390(1)	12.403(2)	2535.3(10)
8	16.494(3)	12.391(2)	12.404(3)	2535.1(15)

We also note that the crystallographic partial occupancy on the Cd3 site [0.174(3); Table 3] may suggest a phase width. Therefore, a series of experiments were designed accordingly with the loading Rb:Cd:Sb ratios of 16:y:36 (y = 20−32) to probe the possible phase width as listed in Table 1. Fortunately, five of these samples, **1**, **4**−**6**, and **8**, produced single crystals with good quality for single-crystal XRD analysis. Also, the refined stoichiometries were $Rb_{16}Cd_{24.94(2)}Sb_{36}$, $Rb_{16}Cd_{25.03(2)}Sb_{36}$, $Rb_{16}Cd_{25.39(3)}Sb_{36}$, $Rb_{16}Cd_{25.47(3)}Sb_{36}$, and $Rb_{16}Cd_{25.46(3)}Sb_{36}$, respectively (Table 5 and the Supporting Information, Table S1). The site occupancies on the Cd3 site (8e) were refined to be 0.117(2), 0.129(2), 0.174(3), 0.184(3), and 0.183(3), respectively (Supporting Information, Table S2), which indicated an increase of the Cd amount. However, such a small increase did not significantly influence the unit cell. The unit cell parameters have been refined from the powder XRD patterns of samples **1**−**6** and **8** with Si as the inner standard to calibrate the systematic error. As listed in Table 6, the results are identical at the 2σ level. We have also refined the single-crystal data with the corresponding "powder unit cell"; the small difference between single-crystal and powder unit cells does not influence the refinement results reported in Tables 2 and 5.

Structure and Bonding. The title compound adopts a novel structure type featuring infinite chains of Rb1-centered dodecahedra, and every four bridged chains define a channel along the c axis that accommodates Rb2, Rb3, and Cd3, as shown in Figure 2. In type I clathrate $Cs_8Cd_{18}Sb_{28}$,[9] the 24-atom tetrakaidecahedra share both trans hexagons so as to form a chain that is running along [100] or [001], respectively. The horizontal and vertical tetrakaidecahedron chains share the side pentagonal faces with the thus-formed intervening 20-atom dodecahedra.[9] Differently, the cage chains in $Rb_{16}Cd_{25.39(3)}Sb_{36}$ are solely constructed by small 20-atom dodecahedra sharing trans pentagons along [001] (Figure 3). Each is connected to four neighboring chains connected via *exo*-Cd2−Sb4 bonds (Figure 3), defining

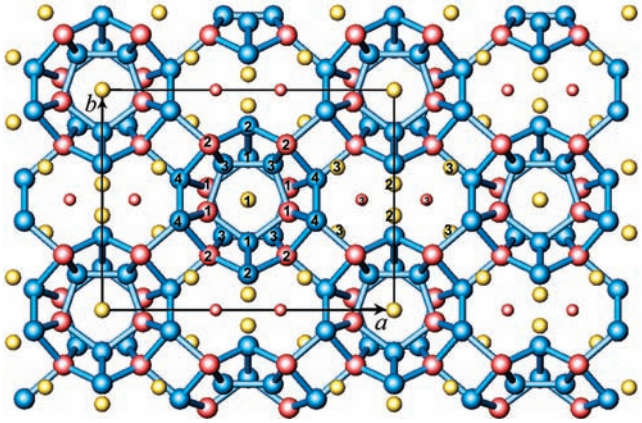

Figure 2. Structure of $Rb_{16}Cd_{25.39(3)}Sb_{36}$ viewed down the *c* axis with the unit cell outlined. Color code: yellow, Rb; red, Cd; blue, Sb. The partially occupied Cd3 atom is shown as a small sphere with the Cd3−Sb bonds omitted for clarity. The bond ranges are for the Cd−Sb bond < 2.95 Å and for the Sb−Sb bond < 2.85 Å.

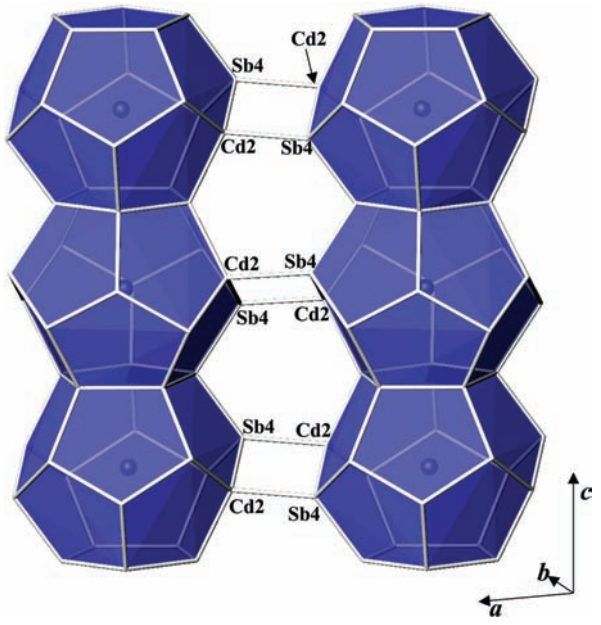

Figure 3. Chains of a Rb1-centered Cd_8Sb_{12} dodecahedron extending along the *c* axis that are connected to each other via *exo*-Cd2−Sb4 bonds of 2.927(1) Å.

the channel, as indicated by Figure 4a, that involves Cd2 and Sb2 atoms and $(Sb4)_2$ dimers.

The Cd_6Sb_{14} dodecahedron in the Sb-based type I clathrate $Cs_8Cd_{18}Sb_{28}$ is centered by Cs1 at the 2*a* site and is constructed by eight Sb atoms from the 16*i* site, six Sb and six Cd from the disordered 24*k* site (shared by Cd and Sb atoms in a 1:1 ratio; Figure S5 in the Supporting Information).[9] However, the mixed occupancy on the 24*k* site blurs the atomic distribution pattern on the skeleton of the dodecahedron. Because Cd with lower electronegativity tends to be a little positive, the Cd−Cd bond is higher in energy than the Cd−Sb bond. Therefore, the Cd−Cd bond is not preferred by the stability of a dodecahedron. To avoid the Cd−Cd bonding interaction, the maximum number of Cd atoms per pentagon face is two (Figure S5 in the Supporting Information). Consequently, the maximum number of Cd atoms per dodecahedron is eight, i.e., 2 (Cd atoms per pentagon face) $\times$ $^1/_3$ (each atom is shared by three pentagon faces) $\times$ 12 (pentagon faces per dodecahedron) = 8. This is what we found in $Rb_{16}Cd_{25.39(3)}Sb_{36}$, in which the Cd_8Sb_{12} dodecahedron consists of 8 Cd atoms and 12 Sb atoms that have full site occupancy (Figure 4b). The simple comparison between clathrate $Cs_8Cd_{18}Sb_{28}$ and $Rb_{16}Cd_{25.39(3)}Sb_{36}$ suggests that such a O_h^2-to-D_{2h}^{17} symmetry decrease destroys the 24-atom tetrakaidecahedron and changes the component of the 20-atom dodecahedron as follows: the disordered 24*k* sites in an O_h^2 dodecahedron (site symmetry: *m*..) have been replaced by four Cd1 at the 8*g* site (..*m*), four Cd2 at the 16*h* site (1), four Sb3 at the 8*g* site (..*m*), and four Sb4 at the 16*h* site (1), while the 16*i* sites in an O_h^2 dodecahedron have been replaced by two Sb1 at the 4*c* site (*m*2*m*) and two Sb2 at the 8*f* site (*m*..). Such an atomic configuration generates a "$Cd_{4+4}Sb_{4+4+2+2}$" dodecahedron without the Cd−Cd bond (Figure 4b). Similarly, we can speculate that in a type I clathrate $Cs_8Cd_{18}Sb_{28}$ each dodecahedron cannot bear more than eight Cd atoms in order to avoid formation of the Cd−Cd bond.

The local coordination environments of Cd and Sb atoms are presented in the Supporting Information, Figure S6. The Cd1 and Cd2 atoms are both tetrahedrally coordinated with the Cd−Sb bond lengths and Sb−Cd−Sb angles that range from 2.825(2)−2.874(2) Å, 107.89(3)−110.24(2)° to 2.833(1)−2.927(1) Å, 91.68(3)−116.69(3)°, respectively (Table 4). These Cd−Sb bond lengths match well with those values in a $CdSb_4$ tetrahedron found in other related compounds, such as Yb_2CdSb_2,[21] Ca_2CdSb_2,[21] $Ba_3Cd_2Sb_4$,[22] $Ba_{21}Cd_4Sb_{18}$,[23] and $Cd_{12.7}Sb_{10}$.[24] The Sb1 and Sb3 atoms are also 4-fold-coordinated in $Sb1Sb_2Cd_2$ and $Sb3Sb_1Cd_3$ tetrahedra, respectively. Also, the Sb2 and Sb4 atoms are 5-fold-coordinated in a Cd_4Sb square-pyramidal motif. The average Sb−Sb bond of 2.827(2) Å is comparable to those found in $Ba_{21}Cd_4Sb_{18}$ [2.824(2) Å],[23] $Sr_{11}Cd_6Sb_{12}$ [2.814(2) Å],[25] $Yb_{11}GaSb_9$ [2.822(2) Å],[26] and $Eu_{11}InSb_9$ [2.823(2) Å][27] but slightly shorter than those in $Eu_5In_2Sb_6$ [2.861(4) Å][28] and $Ca_{21}Mn_4Sb_{18}$ [2.866(1) Å].[29]

As was already mentioned above, the occupancy of 17.4(3)% for the Cd3 site is low; such a partial occupancy on the Cd site is also found in other Cd-containing antimonides. For example, in $Sr_9Cd_{4.49(1)}Sb_9$, the occupancy of Cd (4*g* site) is 0.246(3).[30] The Cd3 site is surrounded by two Sb2 atoms at 2.879(2) Å and a $(Sb4)_2$ dimer at 2.927(3) Å, which matches well with the typical Cd−Sb bond

(21) Xia, S. Q.; Bobev, S. *J. Am. Chem. Soc.* **2007**, *129*, 4049–4057.
(22) Saparov, B.; Xia, S. Q.; Bobev, S. *Inorg. Chem.* **2008**, *47*, 11237–11244.
(23) Xia, S. Q.; Bobev, S. *Inorg. Chem.* **2008**, *47*, 1919–1921.
(24) Zelinska, O. Y.; Bie, H. Y.; Mar, A. *Chem. Mater.* **2007**, *19*, 1518–1522.
(25) Park, S. M.; Kim, S. J. *J. Solid State Chem.* **2004**, *177*, 3418–3422.
(26) Bobev, S.; Fritsch, V.; Thompson, J. D.; Sarrao, J. L.; Eck, B.; Dronskowski, R.; Kauzlarich, S. M. *J. Solid State Chem.* **2005**, *178*, 1071–1079.
(27) Xia, S. Q.; Hullmann, J.; Bobev, S.; Ozbay, A.; Nowak, E. R.; Fritsch, V. *J. Solid State Chem.* **2007**, *180*, 2088–2094.
(28) Park, S. M.; Choi, E. S.; Kang, W.; Kim, S. J. *J. Mater. Chem.* **2002**, *12*, 1839–1843.
(29) Holm, A. P.; Olmstead, M. M.; Kauzlarich, S. M. *Inorg. Chem.* **2003**, *42*, 1973–1981.
(30) Xia, S. Q.; Bobev, S. *J. Am. Chem. Soc.* **2007**, *129*, 10011–10018.

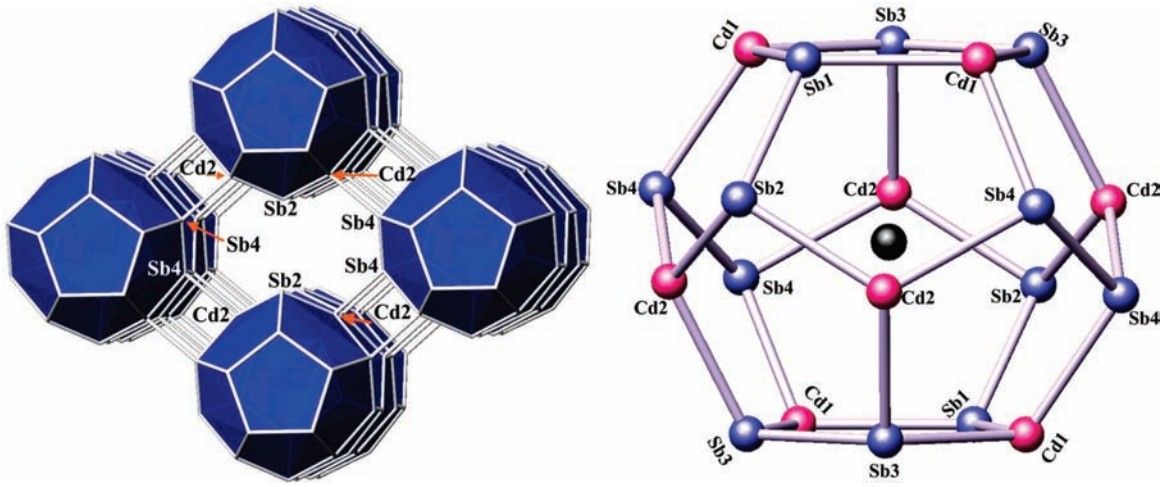

Figure 4. (a) Slightly off-[001] view of the channel defined by Cd2, Sb2, and Sb4. (b) View of the Rb1-centered Cd_8Sb_{12} dodecahedron in $Rb_{16}Cd_{25.39(3)}Sb_{36}$ with atoms marked. Color code: black, Rb1.

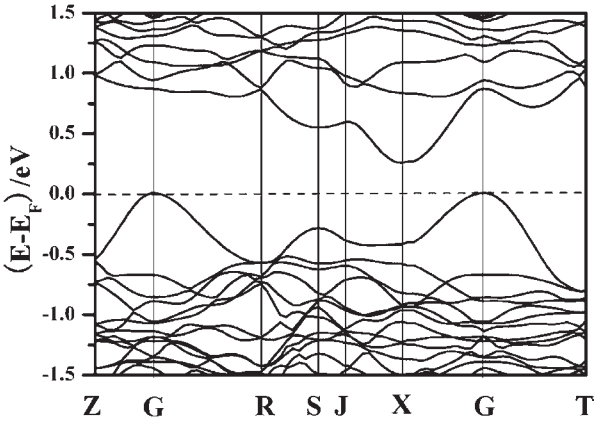

Figure 5. Calculated band structure of the hypothetical model "$[Rb_{16}Cd_{24}Sb_{36}] + 4e$" (II).

length [2.822(2)−3.054(1) Å].[26,31,32] The Sb−Cd−Sb angles vary between 57.66(7) and 139.36(5)°, indicating an extreme distortion. To simplify, if the Cd3−Sb bonding interactions are not taken into account, a 10-membered-ring channel along the *c* axis can be outlined (Figures 2 and 4a), which are constructed by four Cd2 atoms, two Sb2 atoms, and two $(Sb4)_2$ pairs. Such a channel accommodates Rb2 (4*c* site) and Rb3 (8*g* site) atoms. According to Slack's concept of a holey semiconducting TE material,[33] the rattling atoms will move inside the holes and thus scatter the thermal phonons, leading to a low lattice thermal conductivity. Therefore, a low thermal conductivity is expected.

Electronic Structures. According to the Zintl−Klemm concept,[34] the Cd atom can be treated as a closed-shell ion Cd^{2+}, and single-bonded (only the Sb−Sb bond is counted) Sb2, Sb3, and Sb4 are assigned as Sb^{2-}, and the two-bonded Sb1 is assigned as Sb^{-}. The formal oxidation states can then be assigned as $(Rb^{+})_{16}(Cd^{2+})_{24+2}(Sb^{-})_4(Sb^{2-})_{32}$ to reach a charge balance. Such a stoichiometry implies that Cd3 should have a site occupancy of 0.25, i.e., 8×1 (8*g* site) + 16×1 (16*h* site) + 8×0.25 (8*e* site) = 26. Such an assignment suggests that the compounds $Rb_{16}Cd_{24+x}Sb_{36}$ [$0.94(2) \le x \le 1.47(3)$] are electron-deficient because the Cd3 site has an occupancy lower than 0.25.

Subsequently, two hypothetical models of "$[Rb_{16}Cd_{24}Sb_{36}]^0$" (I) and "$[Rb_{16}Cd_{24}Sb_{36}] + 4e$" (II) are proposed in which the single-crystal data are adopted with exclusion of the partially occupied Cd3 atoms. For model II, four additional electrons were added by the rigid-band approximation according to the previous reports.[30,35,36] The band structure of model II plotted in Figure 5 shows a computationally small indirect band gap of 0.23 eV. The densities of states (DOSs) of both I and II are presented in Figure 6. Below the Fermi level, down to −5 eV, the valence bands are dominated by Cd 5s and Sb 5p orbitals with minor contributions of Cd 5p, while above the Fermi level, the conduction bands are mainly Sb 5p orbitals, which hybridize with Rb 4d, Cd 5s, and Cd 5p orbitals. As expected from the Zintl−Klemm concept, Rb, whose contribution to the valence band is negligible, has lost almost entirely its outermost electrons and mostly contributes to the unoccupied DOSs area. Compared with model II, the Fermi energy of model I descends by nearly 0.4 eV and falls in a region of occupied DOS, which suggests a metallic behavior. According to the stoichiometry, the Fermi levels of the compounds $Rb_{16}Cd_{24+x}Sb_{36}$ [$0.94(2) \le x \le 1.47(3)$] are expected to be located between those of models I and II and to exhibit as either a poor metallic conductor or a narrow-band-gap semiconductor. The resistivity measurements on $Rb_{16}Cd_{25.39(3)}Sb_{36}$ (Figure 7) indicate a semiconductor behavior that is in agreement with the calculation.

Electrical and Thermal Transport Properties. The TE property of the polycrystalline pellet of $Rb_{16}Cd_{25.39(3)}Sb_{36}$ was measured as a function of the temperature. As depicted in Figure 7, the electrical conductivity varies nearly linearly with the temperature and features a semiconductor behavior with moderate conductivities of about 39.2 and 57.4 S/cm at

(31) Tkachuk, A. V.; Zelinska, O. Y.; Mar, A. *J. Solid State Chem.* **2006**, *179*, 1506–1512.
(32) Shevelkov, A. V.; Dikarev, E. V.; Popovkin, B. A. *J. Solid State Chem.* **1991**, *93*, 331–335.
(33) Tritt, T. M. *Science* **1999**, *283*, 804–805.
(34) Papoian, G. A.; Hoffmann, R. *Angew. Chem., Int. Ed.* **2000**, *39*, 2409–2448.
(35) Assoud, A.; Thomas, S.; Sutherland, B.; Zhang, H. Q.; Tritt, T. M.; Kleinke, H. *Chem. Mater.* **2006**, *18*, 3866–3872.
(36) Cui, Y. J.; Assoud, A.; Kleinke, H. *Inorg. Chem.* **2009**, *48*, 5313–5319.

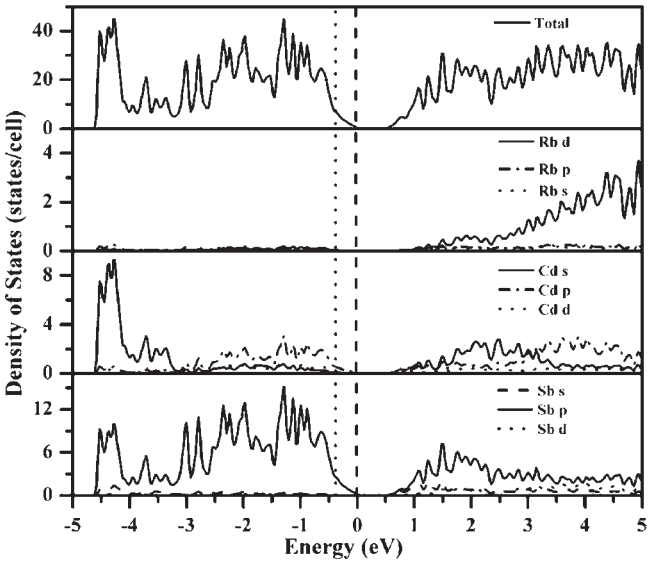

Figure 6. Total and partial DOSs for the hypothetical models of "$[Rb_{16}Cd_{24}Sb_{36}]^{0}$" (I) and "$[Rb_{16}Cd_{24}Sb_{36}] + 4e$" (II). The obvious difference between these models is the location of the Fermi levels: dotted, I; dashed, II.

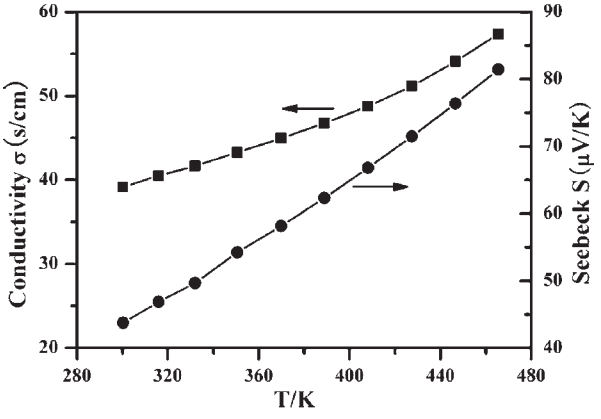

Figure 7. Temperature dependence of the electrical conductivity and Seebeck coefficient for a cold-pressed polycrystalline pellet of $Rb_{16}Cd_{25.39(3)}Sb_{36}$.

300 and 466 K, respectively. Those values are comparable with the room temperature electrical conductivity of ~65 S/cm in the tunnel structure Zintl-phase $BaGa_2Sb_2$[3] but slightly lower than 135 S/cm in the layered Zintl-phase $Ba_4In_8Sb_{16}$.[37] The Seebeck coefficient (S) of $Rb_{16}Cd_{25.39(3)}Sb_{36}$ is about +43.7 μV/K at room temperature, increases almost linearly with an increase in the temperature, and reaches 81.4 μV/K at 466 K. The values are comparable with +65 μV/K in $BaGa_2Sb_2$[3] and 70 μV/K in $Ba_4In_8Sb_{16}$.[37] The positive sign of S indicates that the majority carriers of $Rb_{16}Cd_{25.39(3)}Sb_{36}$ are holes. The thermal conductivity k is nearly temperature-independent and reads as 0.49 W/m·K at room temperature, which is lower than that of the optimized Bi_2Te_3 alloy (1.4–1.6 W/m·K). The low thermal conductivity may be due to the rattling of Rb^+ cations, the presence of heavy metals, and the complex crystal structure of the compound. All of these data generate the TE figure of merit (ZT) for the cold-pressed polycrystalline $Rb_{16}Cd_{25.39(3)}Sb_{36}$ pellet, which

(37) Kim, S. J.; Hu, S. Q.; Uher, C.; Kanatzidis, M. G. *Chem. Mater.* **1999**, *11*, 3154–3159.

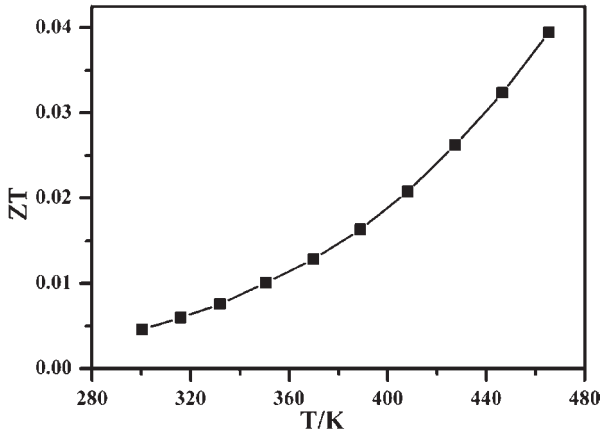

Figure 8. Temperature dependence of the figure of merit (ZT) of $Rb_{16}Cd_{25.39(3)}Sb_{36}$.

increase from 0.0046 at 300 K to 0.04 at 466 K, as plotted in Figure 8. These values may be improved in several ways, such as using a denser pellet made by hot-pressing, doping, or modification of the constituent component, etc.

Conclusions

A new ternary antimonide $Rb_{16}Cd_{25.39(3)}Sb_{36}$ has been synthesized and characterized with a novel polyanion framework constructed by the parallel infinite chains of a Rb^+-centered Cd_8Sb_{12} dodecahedron along the [001] direction. The loading ratio and annealing temperature highly influence the formation of the compound. The Cd_8Sb_{12} dodecahedron, with each skeleton site fully occupied by a certain atom, defines an energetically favored atomic distribution pattern without the Cd−Cd bonding interaction in the polyhedron. A very small phase width $Rb_{16}Cd_{24+x}Sb_{36}$ [$0.94(2) \leq x \leq 1.47(3)$] is due to the partial occupancy on the Cd3 site, which does not significantly influence the unit cell. The TE property measurements on the as-synthesized $Rb_{16}Cd_{25.39(3)}Sb_{36}$ polycrystalline cold-pressed pellet reveal the temperature-dependent electrical conductivity, Seebeck coefficient, and figure of merit (ZT). The thermal conductivity is nearly temperature-independent. The ZT value reaches 0.04 at 466 K. Such a semiconducting behavior agrees well with the results of the first principle calculations. The improvement of the TE property of the title compound via doping or modification of the constituent components is worth the effort. Also, given their chemical similarity, Mn- or Zn-containing analogues are also possible.

Acknowledgment. This research was supported by the National Natural Science Foundation of China under Projects 90922021, 20773130, 20733003, 20821061, and 20973175, the Knowledge Innovation Program of the Chinese Academy of Sciences (Grant KJCX2-YW-H20), and the Key Project from the Chinese Academy of Sciences (Grant KJCX2-YW-H01).

Supporting Information Available: CIF files, powder XRD patterns, view of the Cd_6Sb_{14} dodecahedron in the type I clathrate $Cs_8Cd_{18}Sb_{28}$, local coordination environments of the Cd and Sb atoms in $Rb_{16}Cd_{25.39(3)}Sb_{36}$, crystallographic data and refinements, atomic coordinates, and anisotropic displacement parameters. This material is available free of charge via the Internet at http://pubs.acs.org.